ICSV14
Cairns • Australia
9-12 July, 2007

ACTIVE NOISE CONTROL WITH A VIRTUAL ACOUSTIC SENSOR IN A PURE-TONE DIFFUSE SOUND FIELD

Danielle J. Moreau, Justin Ghan, Ben S. Cazzolato and Anthony C. Zander

School of Mechanical Engineering, the University of Adelaide
SA 5005, Australia
danielle.moreau@mecheng.adelaide.edu.au

Abstract

Local active noise control systems can be used to generate a zone of quiet at a physical error sensor using one or more secondary sources to cancel the acoustic pressure and its spatial derivatives at the sensor location. The resulting zone of quiet is generally limited in size and as such, placement of the physical error sensor at the location of desired attenuation is required, which is often inconvenient. Virtual acoustic sensors overcome this by projecting the zone of quiet away from the physical error sensor to a remote location. The work described here investigates the effectiveness of using virtual microphones and virtual acoustic energy density sensors in a diffuse sound field. Expressions for the performance of the virtual microphones and virtual acoustic energy density sensors have been developed using the forward-difference extrapolation technique which has been rederived for use in diffuse sound fields. Results from simulations will be presented, together with experimental results obtained in a reverberant chamber.

1. INTRODUCTION

Local noise control strategies reduce the sound field at a number of points to create localised zones of quiet at the error sensors. While achieving significant attenuation at the error sensor, the zone of quiet is generally small and impractically sized. Elliott et al. [1] investigated the spatial extent of the zone of quiet when controlling pressure with a remote secondary source in a pure-tone diffuse sound field. The zone of quiet generated at the microphone was found to be defined by a *sinc* function, with the primary sound level reduced by 10 dB over a sphere of diameter one tenth of the excitation wavelength, $\lambda/10$. Attempting to broaden the zone of quiet, Elliott and Garcia–Bonito [2] extended previous theory to the control of both pressure and pressure gradient in a diffuse sound field with two secondary sources. Minimising both the pressure and pressure gradient along a single axis produced a 10 dB zone of quiet over a distance of half a wavelength, $\lambda/2$, in the direction of pressure gradient measurement. This is considerably larger than the zone of quiet obtained when minimising pressure alone.

Virtual sensors are sometimes used in active noise control systems to shift the zone of quiet to a location that is remote from the physical sensor. Garcia-Bonito and Elliott [3] and Garcia-Bonito et al. [4] investigated the performance of virtual sensors in a diffuse sound field using the virtual microphone arrangement [5]. It was demonstrated that the virtual

microphone projects the zone of quiet away from the physical microphone to the location of desired attenuation. This virtual sensing strategy, however, uses the often invalid assumption of equal primary pressure at the physical and virtual locations, which the remote microphone technique overcomes [6]. The forward-difference extrapolation technique [7] is an alternative virtual sensing method that has several advantages. Firstly the assumption of equal primary pressure at the physical and virtual locations does not have to be made but also FIR filters or preliminary identification is not required.

In this paper, optimal prediction algorithms for forward-difference virtual sensors in a diffuse sound field are derived. Since the assumptions made previously [7] when developing this virtual sensing technique are not valid in a diffuse sound field due to the short correlation lengths, this extrapolation method is derived specific to diffuse sound fields. One-dimensional virtual microphones and virtual energy density sensors that use both pressure and pressure gradient sensors are developed with this technique. The performance of these virtual sensors is then explored through numerically simulated and post-processed experimental control.

2. THEORY

In this section, stochastically optimal prediction algorithms for the forward-difference virtual microphones and virtual energy density sensors in a diffuse sound field are derived.

For the present study, the primary and secondary acoustic fields are considered diffuse. The pressure at a position $\boldsymbol{x}$ in a single diffuse acoustic field is denoted $p_i(\boldsymbol{x})$ and $g_i(\boldsymbol{x})$ denotes the x-axis component of the pressure gradient. In the following pages, the subscript i refers to a single diffuse acoustic field, whereas a lack of subscript indicates the total acoustic field produced by superposition of the primary and secondary diffuse acoustic fields.

For a displacement vector, $\mathbf{r} = r_x\mathbf{i}+r_y\mathbf{j}+r_z\mathbf{k}$, the following functions are defined:

$$\mathrm{A}(\mathbf{r}) = \mathrm{sinc}(k|\mathbf{r}|), \tag{1}$$

$$\mathrm{B}(\mathbf{r}) = \frac{\partial\,\mathrm{A}(\mathbf{r})}{\partial r_x} = -k\left(\frac{\mathrm{sinc}(k|\mathbf{r}|)-\cos(k|\mathbf{r}|)}{k|\mathbf{r}|}\right)\left(\frac{r_x}{|\mathbf{r}|}\right), \tag{2}$$

$$\mathrm{C}(\mathbf{r}) = \frac{\partial^2\,\mathrm{A}(\mathbf{r})}{\partial^2 r_x} = -k^2\left[\mathrm{sinc}(k|\mathbf{r}|)\left(\frac{r_x}{|\mathbf{r}|}\right)^2+\left(\frac{\mathrm{sinc}(k|\mathbf{r}|)-\cos(k|\mathbf{r}|)}{(k|\mathbf{r}|)^2}\right)\left(1-3\left(\frac{r_x}{|\mathbf{r}|}\right)^2\right)\right], \tag{3}$$

where k is the wavenumber. The correlations between the pressures and pressure gradients at two different points, $\boldsymbol{x}_j$ and $\boldsymbol{x}_k$, separated by $\mathbf{r}$, are given by [2]

$$\left\langle p_i(\boldsymbol{x}_j)p_i^*(\boldsymbol{x}_k)\right\rangle = \mathrm{A}(\mathbf{r})\left\langle|p_i|^2\right\rangle, \tag{4}$$

$$\left\langle p_i(\boldsymbol{x}_j)g_i^*(\boldsymbol{x}_k)\right\rangle = -\mathrm{B}(\mathbf{r})\left\langle|p_i|^2\right\rangle, \tag{5}$$

$$\left\langle g_i(\boldsymbol{x}_j)p_i^*(\boldsymbol{x}_k)\right\rangle = \mathrm{B}(\mathbf{r})\left\langle|p_i|^2\right\rangle, \tag{6}$$

$$\left\langle g_i(\boldsymbol{x}_j)g_i^*(\boldsymbol{x}_k)\right\rangle = C(\mathbf{r})\left\langle|p_i|^2\right\rangle, \tag{7}$$

where $\langle\cdot\rangle$ denotes spatial averaging. In the case that $\boldsymbol{x}_j$ and $\boldsymbol{x}_k$ are at the same point, the limits of $\mathrm{A}(\mathbf{r})$, $\mathrm{B}(\mathbf{r})$ and $\mathrm{C}(\mathbf{r})$ as $\mathbf{r}\to 0$ must be taken.

If there are m sensors in the field, each measuring pressure or pressure gradient, then define $\mathbf{p}$ as an $m\times 1$ matrix whose elements are the relevant pressures and pressure gradients measured by the sensors. The pressure and pressure gradient at any point can be expressed as the weighted sum of the m components, each of which are perfectly correlated with a corresponding element of $\mathbf{p}$ and a component which is perfectly uncorrelated with each of the elements. Therefore, for each position $\boldsymbol{x}$, $p(\boldsymbol{x})$ and $g(\boldsymbol{x})$ can be written as

$$p(\boldsymbol{x}) = \mathbf{H}_p(\boldsymbol{x})\mathbf{p} + p_u(\boldsymbol{x}), \quad (8) \qquad g(\boldsymbol{x}) = \mathbf{H}_g(\boldsymbol{x})\mathbf{p} + g_u(\boldsymbol{x}), \quad (9)$$

where $\mathbf{H}_p(\boldsymbol{x})$ and $\mathbf{H}_g(\boldsymbol{x})$ are matrices of weights which are functions of the position $\boldsymbol{x}$ only and $p_u(\boldsymbol{x})$ and $g_u(\boldsymbol{x})$ are perfectly uncorrelated with the elements of $\mathbf{p}$. It can be shown, by postmultiplying the expressions for $p(\boldsymbol{x})$ and $g(\boldsymbol{x})$ by $\mathbf{p}^H$ and spatially averaging, that

$$\mathbf{H}_p(\boldsymbol{x}) = \mathbf{L}_p(\boldsymbol{x})\mathbf{M}^{-1}, \quad (10) \qquad \mathbf{H}_g(\boldsymbol{x}) = \mathbf{L}_g(\boldsymbol{x})\mathbf{M}^{-1}, \quad (11)$$

where

$$\mathbf{L}_p(\boldsymbol{x}) = \frac{\left\langle p_i(\boldsymbol{x})\mathbf{p}_i^H \right\rangle}{\left\langle |p_i|^2 \right\rangle}, \quad (12) \qquad \mathbf{L}_g(\boldsymbol{x}) = \frac{\left\langle g_i(\boldsymbol{x})\mathbf{p}_i^H \right\rangle}{\left\langle |p_i|^2 \right\rangle}, \quad (13)$$

$$\mathbf{M} = \frac{\left\langle \mathbf{p}_i \mathbf{p}_i^H \right\rangle}{\left\langle |p_i|^2 \right\rangle}. \quad (14)$$

The aim here is to estimate the pressure and pressure gradient at a virtual location. In order to do this, $p(\boldsymbol{x})$ and $g(\boldsymbol{x})$ must be estimated from the known quantities in $\mathbf{p}$. The pressure and pressure gradient at any point $\boldsymbol{x}$ are given by Equations 8 and 9. If only the measured quantities in $\mathbf{p}$ are known, then the best possible estimates of $p_u(\boldsymbol{x})$ and $g_u(\boldsymbol{x})$ are zero, since they are perfectly uncorrelated with the measured signals. Therefore the best estimates of pressure and pressure gradient at any point $\boldsymbol{x}$ are given by

$$\hat{p}(\boldsymbol{x}) = \mathbf{H}_p(\boldsymbol{x})\mathbf{p}, \quad (15) \qquad \hat{g}(\boldsymbol{x}) = \mathbf{H}_g(\boldsymbol{x})\mathbf{p}. \quad (16)$$

In this paper, the following control strategies are analysed in a diffuse sound field:

1. A single secondary source minimising the pressure at a virtual location estimated using the pressure and pressure gradient at a point.
2. A single secondary source minimising the pressure at a virtual location estimated using the pressures at two closely spaced points.
3. Two secondary sources minimising the pressure and pressure gradient at a virtual location using the pressures and pressure gradients at two closely spaced points.
4. Two secondary sources minimising the pressure and pressure gradient at a virtual location using the pressures at four closely spaced points.

In each of the four control strategies above, the virtual quantities are estimated using Equations 15 and 16. This requires matrix $\mathbf{p}$ whose elements are the relevant pressures and pressure gradients measured by the sensors and calculation of the weight matrices $\mathbf{H}_p(\boldsymbol{x})$ and $\mathbf{H}_g(\boldsymbol{x})$ using matrices $\mathbf{L}_p(\boldsymbol{x})$, $\mathbf{L}_g(\boldsymbol{x})$ and $\mathbf{M}$ defined in Equations 12 - 14.

2.1 Theoretical lower bound for the relative change in mean squared pressure

For each of the four control strategies, the lower bound for the relative change in mean squared pressure can be found as a function of α, the increase in mean squared pressure after control. The variable α is defined as

$$\alpha = \frac{<|p|^2>}{<|p_p|^2>}, \quad (17)$$

where $<|p|^2>$ is the mean squared pressure of the total acoustic field and since all fields are

diffuse, is equal to the sum of the mean squared pressure of the primary acoustic field, $\langle|p_p|^2\rangle$, and the mean squared pressures of acoustic fields due to the secondary sources, $\langle|p_s|^2\rangle$. Elliott et al. [1] demonstrated that when minimising the pressure with a single control source, the random variable $\beta = \langle|p_s|^2\rangle/\langle|p_p|^2\rangle$ has an $F_{2,2}$ distribution. As the variable α can be defined as $\alpha = 1 + \beta$, substitution of $\beta = \alpha - 1$ into the $F_{2,2}$ distribution gives the cumulative distribution function for α as

$$F_{\alpha,1} = \frac{\alpha - 1}{\alpha}. \tag{18}$$

The expressions for the lower bound on the mean squared pressure present a worse case scenario and are summarised as follows [8]:

1. One control source cancelling the pressure at $\boldsymbol{x}_0$, estimated using the pressure and pressure gradient at $\boldsymbol{x}_1$:

$$\frac{\left\langle|p(\boldsymbol{x})|^2\right\rangle}{\left\langle|p_p(\boldsymbol{x})|^2\right\rangle} \leq \left[2\left(\frac{\mathrm{A}(\boldsymbol{x}-\boldsymbol{x}_1)\,\mathrm{B}(\boldsymbol{x}_0-\boldsymbol{x}_1) - \mathrm{B}(\boldsymbol{x}-\boldsymbol{x}_1)\,\mathrm{A}(\boldsymbol{x}_0-\boldsymbol{x}_1)}{\mathrm{B}(\boldsymbol{x}_0-\boldsymbol{x}_1)}\right)^2 + \left(1 - \mathrm{A}^2(\boldsymbol{x}-\boldsymbol{x}_1) - \frac{3}{k^2}\mathrm{B}^2(\boldsymbol{x}-\boldsymbol{x}_1)\right)\right]\alpha. \tag{19}$$

2. One control source cancelling the pressure at $\boldsymbol{x}_0$, estimated using the pressures at $\boldsymbol{x}_1$ and $\boldsymbol{x}_2$:

$$\frac{\left\langle|p(\boldsymbol{x})|^2\right\rangle}{\left\langle|p_p(\boldsymbol{x})|^2\right\rangle} \leq \left[2\left(\frac{\mathrm{A}(\boldsymbol{x}-\boldsymbol{x}_1)\,\mathrm{A}(\boldsymbol{x}_0-\boldsymbol{x}_2) - \mathrm{A}(\boldsymbol{x}-\boldsymbol{x}_2)\,\mathrm{A}(\boldsymbol{x}_0-\boldsymbol{x}_1)}{\mathrm{A}(\boldsymbol{x}_0-\boldsymbol{x}_2) - \mathrm{A}(\boldsymbol{x}_1-\boldsymbol{x}_2)\,\mathrm{A}(\boldsymbol{x}_0-\boldsymbol{x}_1)}\right)^2 + \left(1 - \frac{\mathrm{A}^2(\boldsymbol{x}-\boldsymbol{x}_1) + \mathrm{A}^2(\boldsymbol{x}-\boldsymbol{x}_2) - 2\,\mathrm{A}(\boldsymbol{x}-\boldsymbol{x}_1)\,\mathrm{A}(\boldsymbol{x}-\boldsymbol{x}_2)\,\mathrm{A}(\boldsymbol{x}_1-\boldsymbol{x}_2)}{1 - \mathrm{A}^2(\boldsymbol{x}_1-\boldsymbol{x}_2)}\right)\right]\alpha. \tag{20}$$

3. Two control sources cancelling the pressure and pressure gradient at $\boldsymbol{x}_0$, estimated using the pressures and pressure gradients at $\boldsymbol{x}_1$ and $\boldsymbol{x}_2$:

$$\begin{aligned}\frac{\left\langle|p(\boldsymbol{x})|^2\right\rangle}{\left\langle|p_p(\boldsymbol{x})|^2\right\rangle} \leq \Bigg[3\Bigg(&\left(H_{pp1}(\boldsymbol{x}) - \left(\frac{H_{pp1}(\boldsymbol{x}_0)H_{gg2}(\boldsymbol{x}_0) - H_{gp1}(\boldsymbol{x}_0)H_{pg2}(\boldsymbol{x}_0)}{H_{pp2}(\boldsymbol{x}_0)H_{gg2}(\boldsymbol{x}_0) - H_{gp2}(\boldsymbol{x}_0)H_{pg2}(\boldsymbol{x}_0)}\right)H_{pp2}(\boldsymbol{x})\right.\\ &\left.-\left(-\frac{H_{pp1}(\boldsymbol{x}_0)H_{gp2}(\boldsymbol{x}_0) - H_{gp1}(\boldsymbol{x}_0)H_{pp2}(\boldsymbol{x}_0)}{H_{pp2}(\boldsymbol{x}_0)H_{gg2}(\boldsymbol{x}_0) - H_{gp2}(\boldsymbol{x}_0)H_{pg2}(\boldsymbol{x}_0)}\right)H_{pg2}(\boldsymbol{x})\right)^2\\ &+\frac{k^2}{3}\Bigg(\left(H_{pg1}(\boldsymbol{x}) - \left(\frac{H_{pg1}(\boldsymbol{x}_0)H_{gg2}(\boldsymbol{x}_0) - H_{gg1}(\boldsymbol{x}_0)H_{pg2}(\boldsymbol{x}_0)}{H_{pp2}(\boldsymbol{x}_0)H_{gg2}(\boldsymbol{x}_0) - H_{gp2}(\boldsymbol{x}_0)H_{pg2}(\boldsymbol{x}_0)}\right)H_{pp2}(\boldsymbol{x})\right.\\ &\left.-\left(-\frac{H_{pg1}(\boldsymbol{x}_0)H_{gp2}(\boldsymbol{x}_0) - H_{gg1}(\boldsymbol{x}_0)H_{pp2}(\boldsymbol{x}_0)}{H_{pp2}(\boldsymbol{x}_0)H_{gg2}(\boldsymbol{x}_0) - H_{gp2}(\boldsymbol{x}_0)H_{pg2}(\boldsymbol{x}_0)}\right)H_{pg2}(\boldsymbol{x})\right)^2\Bigg)\\ &+\left(1 - \mathbf{L}_p(\boldsymbol{x})\mathbf{M}^{-1}\mathbf{L}_p^{\mathrm{H}}(\boldsymbol{x})\right)\Bigg]\alpha,\end{aligned} \tag{21}$$

using $\mathbf{H}_p(\boldsymbol{x}) = \begin{bmatrix} H_{pp1}(\boldsymbol{x}) \\ H_{pp2}(\boldsymbol{x}) \\ H_{pg1}(\boldsymbol{x}) \\ H_{pg2}(\boldsymbol{x}) \end{bmatrix}$ and $\mathbf{H}_{\mathrm{g}}(\boldsymbol{x}) = \begin{bmatrix} H_{gp1}(\boldsymbol{x}) \\ H_{gp2}(\boldsymbol{x}) \\ H_{gg1}(\boldsymbol{x}) \\ H_{gg2}(\boldsymbol{x}) \end{bmatrix}$.

4. Two control sources cancelling the pressure and pressure gradient at $\boldsymbol{x}_0$, estimated using the pressures at $\boldsymbol{x}_1$, $\boldsymbol{x}_2$, $\boldsymbol{x}_3$ and $\boldsymbol{x}_4$:

$$\frac{\left\langle |p(\boldsymbol{x})|^2 \right\rangle}{\left\langle |p_p(\boldsymbol{x})|^2 \right\rangle} \leq \Bigg[3\Bigg(\Bigg(H_{pp1}(\boldsymbol{x}) - \left(\frac{-H_{pp1}(\boldsymbol{x}_0)H_{gp4}(\boldsymbol{x}_0) + H_{gp1}(\boldsymbol{x}_0)H_{pp4}(\boldsymbol{x}_0)}{\left(-H_{pp3}(\boldsymbol{x}_0)H_{gp4}(\boldsymbol{x}_0) + H_{gp3}(\boldsymbol{x}_0)H_{pp4}(\boldsymbol{x}_0)\right)} \right) H_{pp3}(\boldsymbol{x}) \\ - \left(\frac{H_{pp1}(\boldsymbol{x}_0)H_{gp2}(\boldsymbol{x}_0) - H_{gp1}(\boldsymbol{x}_0)H_{pp2}(\boldsymbol{x}_0)}{\left(-H_{pp3}(\boldsymbol{x}_0)H_{gp4}(\boldsymbol{x}_0) + H_{gp3}(\boldsymbol{x}_0)H_{pp4}(\boldsymbol{x}_0)\right)} \right) H_{pp4}(\boldsymbol{x}) \Bigg)^2 \\ + \frac{k^2}{3} \Bigg(H_{pp2}(\boldsymbol{x}) - \left(\frac{-H_{pp2}(\boldsymbol{x}_0)H_{gp4}(\boldsymbol{x}_0) + H_{gp2}(\boldsymbol{x}_0)H_{pp4}(\boldsymbol{x}_0)}{\left(-H_{pp3}(\boldsymbol{x}_0)H_{gp4}(\boldsymbol{x}_0) + H_{gp3}(\boldsymbol{x}_0)H_{pp4}(\boldsymbol{x}_0)\right)} \right) H_{pp3}(\boldsymbol{x}) \\ - \left(\frac{H_{pp2}(\boldsymbol{x}_0)H_{gp3}(\boldsymbol{x}_0) - H_{gp2}(\boldsymbol{x}_0)H_{pp3}(\boldsymbol{x}_0)}{\left(-H_{pp3}(\boldsymbol{x}_0)H_{gp4}(\boldsymbol{x}_0) + H_{gp3}(\boldsymbol{x}_0)H_{pp4}(\boldsymbol{x}_0)\right)} \right) H_{pp4}(\boldsymbol{x}) \Bigg)^2 \Bigg) \\ + \left(1 - \mathbf{L}_p(\boldsymbol{x})\mathbf{M}^{-1}\mathbf{L}_p^{\mathrm{H}}(\boldsymbol{x})\right) \Bigg] \alpha, \tag{22}$$

using $\mathbf{H}_p(\boldsymbol{x}) = \begin{bmatrix} H_{pp1}(\boldsymbol{x}) \\ H_{pp2}(\boldsymbol{x}) \\ H_{pp3}(\boldsymbol{x}) \\ H_{pp4}(\boldsymbol{x}) \end{bmatrix}$ and $\mathbf{H}_{\mathrm{g}}(\boldsymbol{x}) = \begin{bmatrix} H_{gp1}(\boldsymbol{x}) \\ H_{gp2}(\boldsymbol{x}) \\ H_{gp3}(\boldsymbol{x}) \\ H_{gp4}(\boldsymbol{x}) \end{bmatrix}$.

3. NUMERICAL AND EXPERIMENTAL VALIDATION

The performance of the four virtual sensor formulations was evaluated using a MATLAB simulation and post-processed experimental data. Quadratic optimisation [9] was used to simulate control using both the numerical model and the experimentally measured transfer functions, giving the limit on the maximum achievable feedforward control performance.

The acoustic field was simulated using the numerical model described by Bullmore et al. [10]. This numerical model assumes that the pressure at any point is calculated using a finite modal summation. The enclosure model used in this simulation was that described by Elliott et al. [1] and was rectangular in shape with dimensions π m $\times$ e m $\times$ 1 m. The constant damping ratio was set to be 0.0014 and the Schroeder frequency [11] was calculated as 400 Hz. An excitation frequency of 1.5 kHz was used and all modes with natural frequencies below 2 kHz were included so that the total number of modes was approximately 8000. A number of sources (dependent on the control strategy) were randomly located within the enclosure such that they were not within a wavelength of one another, or the enclosure walls. The average mean squared pressure [1] of the total controlled pressure field was computed over 200 source configurations at various distances in the x-direction from the point of cancellation.

Post-processed control was implemented computationally using transfer functions experimentally measured in the reverberation chamber in the School of Mechanical Engineering at the University of Adelaide. The chamber has dimensions 6.840 m $\times$ 5.660 m $\times$ 4.720 m, a volume of V = 183 m^3 and a Schroeder frequency [11] of 391 Hz. Six loudspeakers were located near the corners of the room allowing a large number of combinations of primary and secondary sources to be used. A condenser microphone and a Microflown, to measure pressure and pressure gradient respectively, were mounted to a stepper-motor traverse enabling measurement over a 465 mm $\times$ 360 mm $\times$ 320 mm volume. The sources were driven with a multi-tonal signal containing tones from 800 Hz to 3000 Hz in 50 Hz increments and the complex transfer functions between each of the sources and the

sensors were measured. Using the averaging procedure described for the simulations, the total controlled pressure field was calculated. In applying post-processed control, the transfer functions between the secondary sources and the sensors were found to be poorly conditioned for certain source and sensor configurations, leading to inaccurate calculation of the optimal control strengths with quadratic optimisation. To improve results, poorly conditioned data sets were not included in the calculation of the mean squared pressure with control.

4. RESULTS

Figure 1 shows the performance of conventional control strategies directly minimising the measured quantities in numerically simulated and post-processed control. The solid vertical lines indicate the positions of the physical sensors. As shown in Figure 1 (a), minimising the pressure at the sensor location with a single control source reduces the primary sound pressure level by 10 dB over a distance of $\lambda/10$, for a value of $\alpha = 2$ (where α is the 50^{th} percentile value). Minimising the pressure and pressure gradient with two control sources extends the 10 dB zone of quiet to $\lambda/2$, for a value of $\alpha = 3.4$, as shown in Figure 1 (b).

Figure 2 shows the control profiles obtained with each of the virtual sensing strategies in a pure-tone diffuse sound field. The zones of quiet generated in numerically simulated and post-processed control are shown, together with the theoretical lower bound for the relative change in mean squared pressure. The dashed vertical line indicates the virtual location.

It is clear from Figure 2 that virtual sensors are capable of projecting the zones of quiet away from the physical sensors to the desired location. Figure 2 (a) shows a comparison of the three evaluation methods when controlling pressure at a virtual location, estimated using the pressure and pressure gradient at a point, for a value of $\alpha = 2$. A maximum attenuation of approximately 23 dB is achieved at the desired location with the numerical model while control predictions using the experimentally measured transfer functions achieved 17 dB of attenuation. A 10 dB reduction in primary sound pressure level is seen over a distance of $\lambda/10$ in both numerically simulated and post-processed control. As expected, both these evaluation methods generate broader zones of quiet than the lower bound on performance. Similar control performance can be obtained using the pressures at two points to estimate the pressure at the virtual location as shown in Figure 2 (b). In comparison to Figure 1, control with a virtual microphone achieves higher levels of attenuation at the virtual location than conventional control strategies employing a single microphone. Using two control sources to minimise the pressure and pressure gradient at the sensor however, achieves higher levels of attenuation at the virtual location than control with a virtual microphone.

The virtual energy density sensors outperform the virtual microphones by generating broader zones of quiet and achieving higher attenuation at the virtual location as seen in Figures 2 (c) and (d). Figure 2 (c) shows the control profiles for cancelling the pressure and pressure gradient at a virtual location, estimated using the pressures and pressure gradients at two points, for a value of $\alpha = 3.4$. Similarly to the virtual microphones, higher attenuation is seen in numerically simulated control with greater than 50 dB achieved, while only 39 dB of attenuation is achieved with post-processed data. A 10 dB zone of quiet of size approximately 0.4λ is generated in both the numerical simulation and post-processed control as opposed to 0.5λ for pressure and pressure gradient control at the physical sensors. As seen previously, the numerical simulation and post-processed control produce larger zones of quiet than the theoretically derived lower bound on performance. Similar control performance can be obtained using the pressures at four points to estimate the pressure and pressure gradient at the virtual location as shown in Figure 2 (d). In comparison to Figure 1, control with a virtual energy density sensor achieves higher levels of attenuation at the virtual location than conventional control strategies employing a single microphone or an energy density sensor.

Figure 3 (a) shows the distribution of α, observed in both numerical and experimental control of pressure at the virtual location with a single secondary source, compared to $F_{\alpha,1}$ given by Equation (18). This distribution is seen to be a good fit with $F_{\alpha,1}$ indicating that control of pressure at either the physical or virtual location results in the same distribution for α. The cumulative distribution function for α when using two secondary sources is shown in Figure 3 (b). It is most likely that the pressure level after control will be higher when using two secondary sources compared to a single secondary source. For example, the median (50th percentile) value of the increase in mean squared pressure after control, α, is approximately 2 for a single control source and 3.4 for two control sources, as shown in Figure 3 (b). The distributions do not have a finite mean value, however, in practice they will be limited by the strengths of the secondary sources.

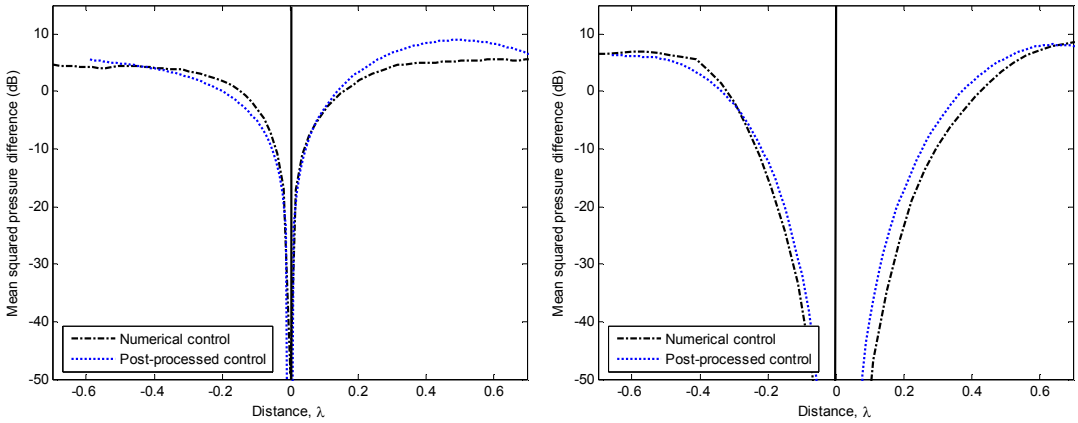

(a) Pressure control (b) Pressure and pressure gradient control

Figure 1. Control profiles obtained with the conventional control strategies.

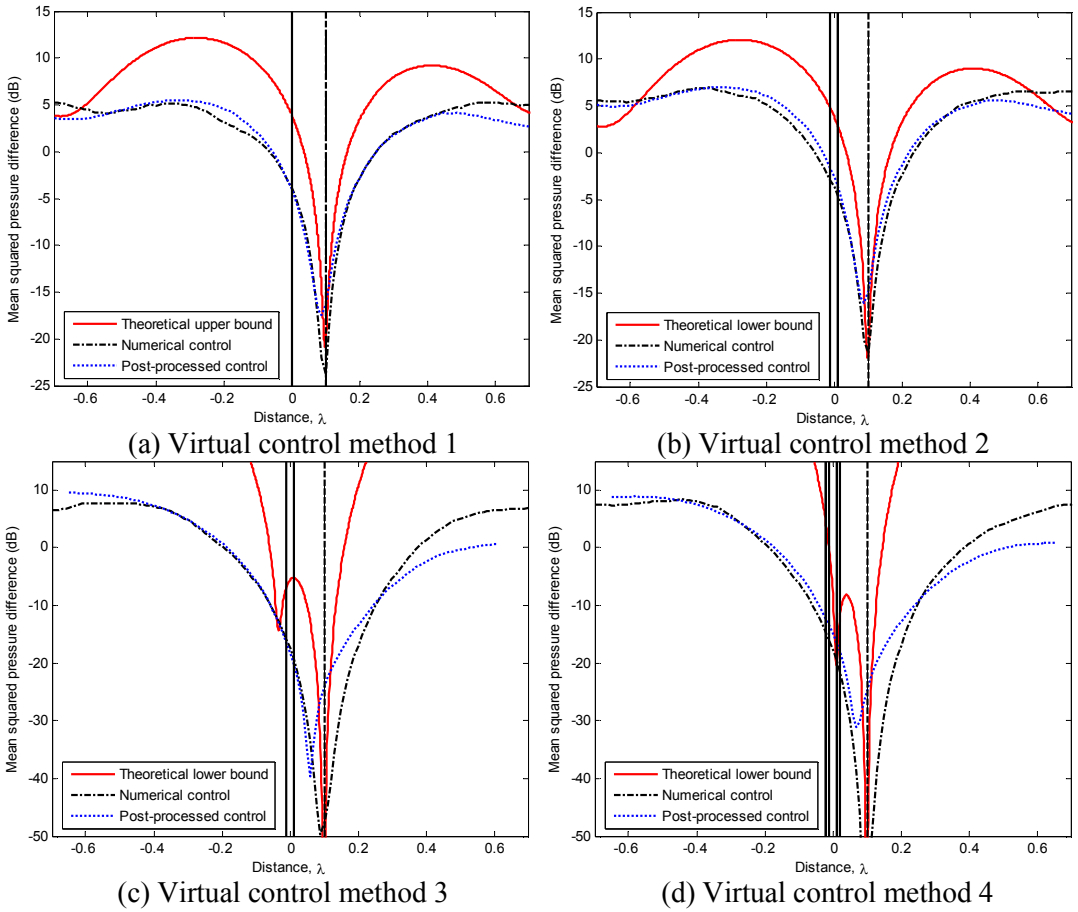

(a) Virtual control method 1 (b) Virtual control method 2

(c) Virtual control method 3 (d) Virtual control method 4

Figure 2. Control profiles obtained with the virtual control strategies.

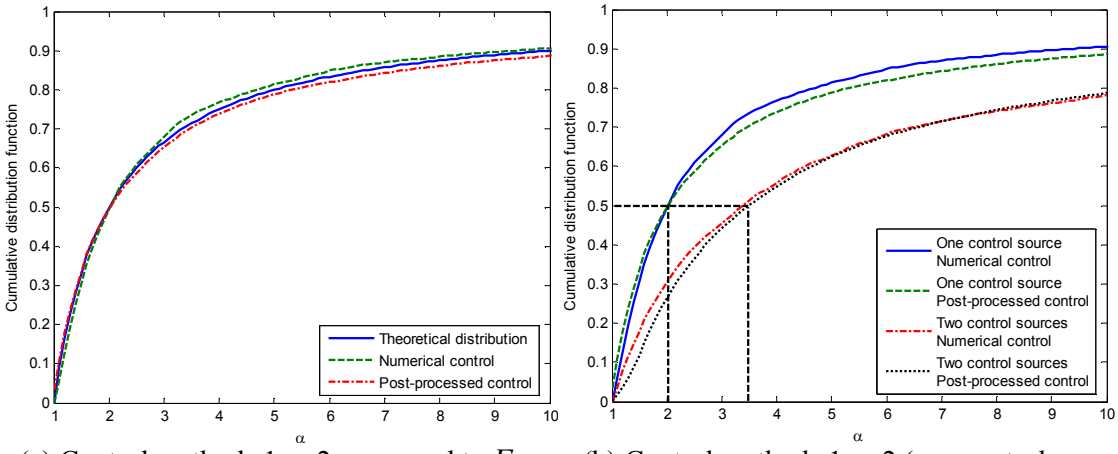

(a) Control methods 1 or 2 compared to $F_{\alpha,1}$ (b) Control methods 1 or 2 (one control source) and 3 or 4 (two control sources)

Figure 3. Cumulative distributions for α.

5. CONCLUSION

Prediction algorithms for forward-difference virtual sensors in a pure-tone diffuse sound field have been derived. Expressions have also been presented for the lower bound on the relative change in mean squared pressure, after cancelling the virtual quantities with remote secondary sources. Results of numerically simulated and post-processed control demonstrated that forward-difference virtual sensors are capable of minimising pressure and pressure gradient at a location that is remote from the physical sensors in a pure-tone diffuse sound field.

REFERENCES

[1] S.J. Elliott, P. Joseph, A.J. Bullmore and P.A. Nelson, "Active cancellation at a point in a pure-tone diffuse sound field", *Journal of Sound and Vibration* **120**(1), 183-189 (1988).

[2] S.J. Elliott and J. Garcia-Bonito, "Active cancellation of pressure and pressure gradient in diffuse sound field", *Journal of Sound and Vibration* **186**(4), 696-704 (1995).

[3] J. Garcia-Bonito and S.J. Elliott, "Strategies for local active control in diffuse sound fields", *Proceedings of Active 95,* 561-572.

[4] J. Garcia-Bonito, S.J. Elliott and C.C. Boucher, "Generation of zones of quiet using a virtual microphone arrangement", *Journal of the Acoustical Society of America* **101**(6), 3498-3516 (1997).

[5] S.J. Elliott and A. David, "A virtual microphone arrangement for local active sound control", *Proceedings of the 1st International Conference on Motion and Vibration Control,* 1027-1031 (1992).

[6] A. Roure and A. Albarrazin, "The remote microphone technique for active noise control", *Proceedings of Active 99*, 1233-1244.

[7] B.S. Cazzolato, "Sensing systems for active control of sound transmission into cavities", *Ph.D. thesis,* Department of Mechanical Engineering, The University of Adelaide, SA (1999).

[8] D.J. Moreau, "Active noise control in three-dimensions using virtual sensors", *Internal Report, Progress Report: Long*, School of Mechanical Engineering, The University of Adelaide, 2007.

[9] S.J. Elliott, *Signal processing for active control,* Academic Press, 2001.

[10] A.J. Bullmore, P.A. Nelson, A. Curtis and S.J. Elliott, "The active minimisation of harmonic enclosed sound fields, part II: A computer simulation", *Journal of Sound and Vibration* **117**(1), 15-33 (1987).

[11] M. Schroeder and K. Kuttruff, "On frequency response curves in rooms, comparison of experimental, theoretical and Monte Carlo results for the average frequency spacing between maxima", *Journal of the Acoustical Society of America* **34**(1), 76-80 (1962).